SAE INTERNATIONAL

ARTICLE INFO
Article ID: 01-16-03-0018

doi:10.4271/01-16-03-0018

The Lynchpin—A Novel Geometry for Modular, Tangential, Omnidirectional Flight

Terrence Dashon Howard,[1] Christian Molter,[2] Chris Dale Seely,[1] and Jeff Yee[3]

[1]Tangential Flight Corporation, USA
[2]University of Stuttgart, Germany
[3]Airwaive, USA

Abstract

A novel geometry for a six degrees of freedom (6DOF) unmanned aerial vehicle (UAV) rotary wing aircraft is introduced and a flight mechanical analysis is conducted for an aircraft built in accordance to the thrust vectors of the proposed geometry. Furthermore, the necessary mathematical operations and control schemes are derived to fly an aircraft with the proposed geometry. A system identification of the used propulsion system with the necessary thrust reversal in the form of bidirectional motors and propellers was conducted at a whirl tower. The design of the first prototype aircraft is presented as well as the first flight test results. It could be demonstrated that an aircraft with the thrust vectors oriented according to the proposed geometry works sufficiently and offers unique maneuvering capabilities that cannot be reached with a conventional design. The biggest limiting factor could be identified to be the latency resulting from the time needed to reverse the direction of rotation of the bidirectional propellers. Special operational handling considerations for a manually flown 6DOF vehicle are summarized, and different approaches to control such a vehicle are described. Different mission scenarios and applications for a single aircraft in this design are concluded. Due to the symmetrical properties of the proposed geometry, several aircraft can also be connected at different orientations in flight. Consequently, the possibilities of docking in midair are illustrated, and possible mission scenarios for a group of aircraft, working together collaboratively, are presented. Especially when operated autonomously in a group of aircraft, new possibilities evolve from the capability of the proposed geometry to bond in different orientations.

History

Received: 03 Dec 2021
Revised: 10 Sep 2022
Accepted: 07 Feb 2023
e-Available: 15 Mar 2023

Keywords

6DOF, Drone, Swarm, Drone mid-air docking, UAV, Flying structures, Lynchpin, Tangential flight, omnidirectional flight, modular drones

Citation

Howard, T., Molter, C., Seely, C., and Yee, J., "The Lynchpin—A Novel Geometry for Modular, Tangential, Omnidirectional Flight," *SAE Int. J. Aerosp.* 16(3):2023, doi:10.4271/01-16-03-0018.

ISSN: 1946-3855
e-ISSN: 1946-3901

This article is a part of a Special Issue on Unmanned Aircraft Systems (UAS) and Autonomy.

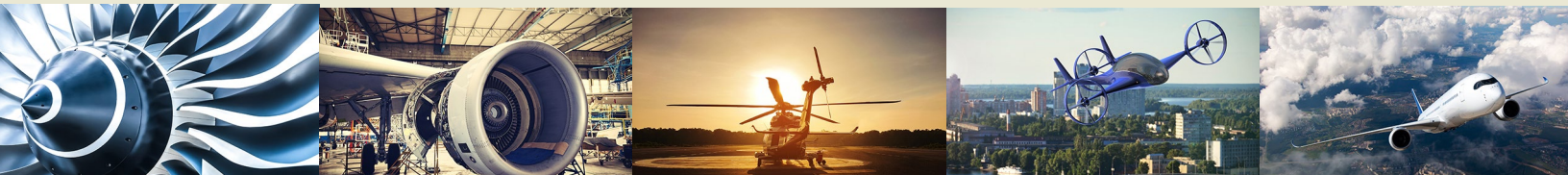

Introduction

For almost all rotary wing aircraft, translational and rotational movements are coupled. By the use of a tiltrotor configuration, it is possible to have an additional degree of freedom (DOF), for example, for the longitudinal axis [1, 2]. Also, tandem helicopters can pitch up or down while hovering to some degree because they have a collective and cyclic pitch at the front and rear rotors [3]. However, pure six degrees of freedom (6DOF) flight has so far not often been used for aviation. An example of a pure 6DOF unmanned aerial vehicle (UAV) is the Omnicopter from ETH Zurich [4]. For the Omnicopter, eight propellers with a reversible direction of rotation and hence reversible thrust have been used to achieve this goal. The orientations of those eight propellers have been determined by numerically solving an optimization problem.

Another 6DOF vehicle that was designed with tiltable propellers, but has never been built, is the holocopter [5].

The authors of this article introduce another geometry which has been inspired by nature in the field of particle physics [6] and, so far, has not been used in aviation. Based on this proposed geometry, a collapsed dodecahedron, called "the Lynchpin" [6, 7], a 6DOF UAV has been designed, built, and tested.

With a 6DOF vehicle, new missions are possible that have not been feasible before. Since, to the knowledge of the authors, the only operational 6DOF vehicle capable of full 360° rotations in space is the Omnicopter [4], there have not been many mission scenarios shown for such a vehicle. However, even a limited rotational DOF offers advantages for inspection and maintenance missions as shown by the VOLIRO AG [8, 9].

SI units are used throughout this article, in common with journal normal practice. However, since the nomenclature for propellers is always in inches, this is an exception to the general rule.

The Lynchpin Geometry

As an icosi-dodecahedron, being a secondary form of an expanded Lynchpin as the a priori fundamental geometrical form in vector equilibrium [10], the Lynchpin consists of six pentagons, as described in Figure 1 and Equation 3, where Equation 3 defines the positions of the corner points shown in Figure 1, and can be derived from four Tetryen elements [6] as shown in Figure 1 on the left side. All dimensions in the pentagons are of length *a*. The Lynchpin is highly symmetric. All six planes in which the pentagons are located are also symmetry planes.

Utilizing the Lynchpin as a 6DOF UAV offers two unique advantages. First, due to its symmetrical properties, it is easy to produce thrust in any direction. Second, the outer shape of the pentagons allows several UAVs to bond in different formations as shown later.

FIGURE 1 The Lynchpin geometry derived from four Tetryen elements [6] as shown on the left.

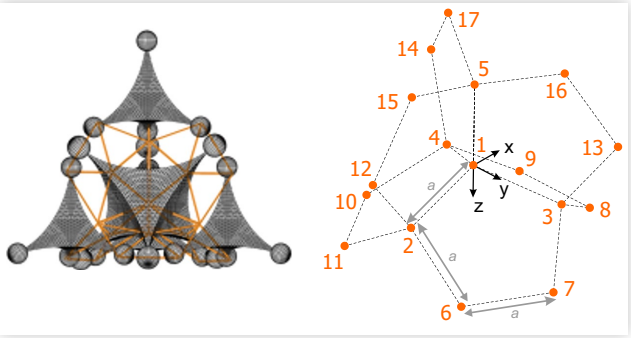

Flight Mechanical Analysis

When using six propellers, one placed inside each of the six pentagons, the results are six linearly independent thrust vectors as shown in Equation 1 and Figure 2.

$$\mathbf{D} = \begin{bmatrix} -\sqrt{1/12} & -\sqrt{1/12} & \sqrt{1/3} & -\sqrt{3/2} & 0 & \sqrt{3/2} \\ 1/2 & -1/2 & 0 & 1/2 & -1 & 1/2 \\ -\sqrt{2/3} & -\sqrt{2/3} & -\sqrt{2/3} & 0 & 0 & 0 \end{bmatrix} \quad \text{Eq. (1)}$$

Thus, we can create a vehicle with six independently controllable DOFs in flight. Equation 2 shows the position of those thrust vectors inside the pentagons, where l is the distance to the origin.

FIGURE 2 Orientations and positions of the six thrust vectors.

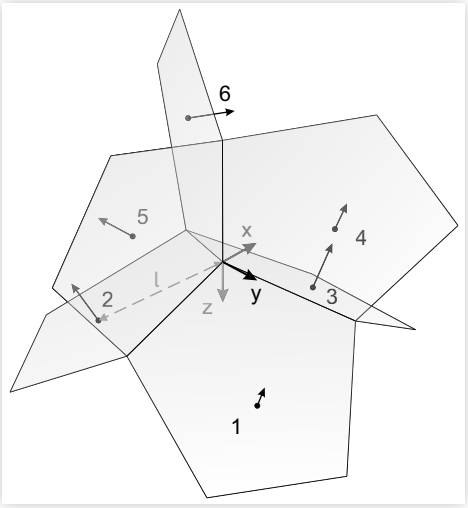

$$\mathbf{P} = l\begin{bmatrix} -\sqrt{1/6} & -\sqrt{1/6} & \sqrt{2/3} & \sqrt{1/6} & -\sqrt{2/3} & \sqrt{1/6} \\ \sqrt{1/2} & -\sqrt{1/2} & 0 & \sqrt{1/2} & 0 & -\sqrt{1/2} \\ \sqrt{1/3} & \sqrt{1/3} & \sqrt{1/3} & -\sqrt{1/3} & -\sqrt{1/3} & -\sqrt{1/3} \end{bmatrix} \quad \text{Eq. (2)}$$

$$\begin{bmatrix} \vec{r}_1^{\,\mathrm{T}} \\ \vdots \\ \vec{r}_{17}^{\,\mathrm{T}} \end{bmatrix} = a\begin{bmatrix} 0 & 0 & 0 \\ -0.9428 & 0 & 0.3333 \\ 0.4714 & 0.8165 & 0.3333 \\ 0.4714 & -0.8165 & 0.3333 \\ 0 & 0 & -1.0000 \\ -1.0560 & 0.8290 & 0.8810 \\ -0.1900 & 1.3290 & 0.8810 \\ 1.2459 & 0.5000 & 0.8810 \\ 1.2459 & -0.5000 & 0.8810 \\ -0.1900 & 1.3290 & 0.8810 \\ -1.0560 & -0.8290 & 0.8810 \\ -1.5346 & 0.0000 & -0.4728 \\ 0.7673 & 1.3290 & -0.4728 \\ 0.7673 & -1.3290 & -0.4728 \\ -0.9573 & 0.0000 & -1.2893 \\ 0.4786 & 0.8290 & -1.2893 \\ 0.4786 & -0.8290 & -1.2893 \end{bmatrix} \quad \text{Eq. (3)}$$

The forces on the aircraft by the rotor thrust vectors can be calculated by

$$\begin{bmatrix} F_x & F_y & F_z \end{bmatrix}^{\mathrm{T}} = \mathbf{D}\begin{bmatrix} T_1 & T_2 & T_3 & T_4 & T_5 & T_6 \end{bmatrix}^{\mathrm{T}} \quad \text{Eq. (4)}$$

where $T_1 \ldots T_6$ are the propeller thrusts in *N*. The moment of the *i*-th propeller on the center of the aircraft (origin axis system in Figure 2) can be calculated as

$$\begin{bmatrix} M_x \\ M_y \\ M_z \end{bmatrix}_i = \mathbf{P}_{*,\mathrm{i}} \times \mathbf{D}_{*,\mathrm{i}} \mathrm{T_i} + \mathbf{D}_{*,\mathrm{i}} \mathrm{Q_i} \quad \text{Eq. (5)}$$

where $\mathbf{P}_{*,\mathrm{i}}$ is the *i*-th column of **P** and $\mathrm{Q_i}$ is the torque of the *i*-th propeller in *Nm*. It is known from basic propeller aerodynamics (compare, e.g., [11]) that the torque of a propeller is proportional to its thrust:

$$\mathrm{Q_i} = \mathrm{k_t T_i} \quad \text{Eq. (6)}$$

The factor $\mathrm{k_t}$ depends on the actual propeller. The direction of rotation can be accounted for with the sign $\mathrm{Q_i}$. Different configurations have been investigated and no advantage could be found by mixing the directions of rotations, and consequently, for the sake of simplicity and availability of spare parts, the direction of rotation for all propellers was chosen as clockwise (CW); hence, for a positive thrust vector in the direction shown in Figure 2, the torque $\mathrm{Q_i}$ becomes negative.

When the center of gravity (CG) is not located exactly at the origin of the aircraft, this offset can be accounted for with a vector $\mathbf{d}_{\mathrm{CG}}$. By summing up the resulting moments of all six propellers on the CG, we get the total moment vector:

$$\begin{bmatrix} M_x \\ M_y \\ M_z \end{bmatrix} = \sum_{i=1}^{6} \left(\left(\mathbf{P}_{*,\mathrm{i}} - \mathbf{d}_{\mathrm{CG}} \right) \times \mathbf{D}_{*,\mathrm{i}} + \mathbf{D}_{*,\mathrm{i}} \mathrm{k_t} \right) \mathrm{T_i} \quad \text{Eq. (7)}$$

When combining Equations 4 and 7 into a matrix **M**, it is possible to express the effect of the six motors on all six forces and moments with one equation:

$$\begin{bmatrix} F_x & F_y & F_z & M_x & M_y & M_z \end{bmatrix}^{\mathrm{T}} = \mathbf{M}\begin{bmatrix} T_1 & \ldots & T_6 \end{bmatrix}^{\mathrm{T}} \quad \text{Eq. (8)}$$

where **M** is

$$\mathbf{M} = \begin{bmatrix} \mathbf{D} \\ \sum_{i=1}^{6} \left(\mathbf{P}_{*,\mathrm{i}} - \mathbf{d}_{\mathrm{CG}} \right) \times \mathbf{D}_{*,\mathrm{i}} + \mathbf{D}_{*,\mathrm{i}} \mathrm{k_t} \end{bmatrix} \quad \text{Eq. (9)}$$

The forces and moments $\begin{bmatrix} F_x & F_y & F_z & M_x & M_y & M_z \end{bmatrix}^{\mathrm{T}}$ correspond to the 6DOF in space. For example, F_x will move the vehicle in the x-direction, while M_x will tilt it about the x-axis. Since **M** is square and non-singular, because the motor directions are linearly independent, it can always be inverted and we can determine how much thrust is needed for each motor to achieve a specific magnitude of forces and moments, hence a specific control input:

$$\begin{bmatrix} T_1 & \ldots & T_6 \end{bmatrix}^{\mathrm{T}} = \mathbf{M}^{-1}\begin{bmatrix} F_x & F_y & F_z & M_x & M_y & M_z \end{bmatrix}^{\mathrm{T}} \quad \text{Eq. (10)}$$

It should be mentioned that, contrary to a regular multirotor aircraft, the z-position of the CG has an impact on the resulting motor thrusts. Therefore, a sensitivity analysis has been conducted.

To investigate how strong this effect is, we set up the matrix $\mathbf{M_{ideal}}^{-1}$ to convert from forces and moments to motor thrusts. The necessary values for *l* and $\mathrm{k_t}$ are taken from the prototype aircraft. For $\mathbf{M_{ideal}}^{-1}$ it is assumed that the CG is located directly at the aircraft origin. Furthermore, we assume that in reality the CG is offset by 42 mm in the negative z-direction, which represents the placement of the flight

FIGURE 3 CAD model of the prototype Lynchpin.

© Tangential Flight Corporation

battery on top of the aircraft instead of the planned location at the bottom (compare Figure 3). For this real CG position, the matrix to convert from motor thrusts back to the vector of forces and moments $\mathbf{M}_{\mathbf{real}}$ is also set up.

Starting with the vector $\begin{bmatrix} 0 & 0 & -mg & 0 & 0 & 0 \end{bmatrix}^{\mathrm{T}}$ for a balanced hovering flight, it can be seen that there is no influence of the CG offset on the motor thrusts in this flight condition. Also, when demanding a pure pitching, rolling, or yawing moment, for example, $\begin{bmatrix} 0 & 0 & -mg & 0 & M & 0 \end{bmatrix}^{\mathrm{T}}$, the changed CG position has only a marginal effect on the motor outputs.

However, a significant influence can be seen when demanding a pure lateral force such as $\begin{bmatrix} mg/2 & 0 & -mg & 0 & 0 & 0 \end{bmatrix}^{\mathrm{T}}$. Here the real output with the CG offset becomes $\begin{bmatrix} mg/2 & 0 & -mg & 0.16mgl & 0 & 0 \end{bmatrix}^{\mathrm{T}}$, which means that there will be a negative rolling moment of the magnitude of 1/7 of L_{max}. This rolling moment will be treated as an external disturbance by the attitude controller and will be compensated for. However, the CG position should be adjusted as close as possible to the designated CG position, for which the motor matrix has been set up.

During flight testing with different battery sizes and an additional payload in the form of a camera, which was not considered when setting up the motor matrix, no problems could be observed. Strategies to handle different CG positions in future applications are a motor matrix that can be adjusted to the payload in the firmware before takeoff or a self-learning algorithm, which observes the actual motor outputs and the vehicle movements to learn the CG offsets, similar to the hover thrust estimator algorithm in the PX4 firmware [12, 13].

In [4] different thrust vector/propeller arrangements for 6DOF flight are presented as a result of a numerical solution to an optimization problem. This algorithm did not find the hexrotor configuration, which is presented here as the "Lynchpin." However, another hexrotor configuration was found. It is pointed out in [4] that, from a purely mathematical point of view, the configuration with only six rotors "is unable to hover at arbitrary attitudes" because "the rotors cannot generate thrusts of arbitrarily small magnitudes." Consequently, the author of [4] decided on an overactuated configuration with eight propellers so that, for the same flight condition, different propeller thrust solutions exist and a state of near-zero thrust can be avoided. This makes it necessary, however, for the flight controller to obtain all possible thrust solutions at all times during flight and decide which one avoids low thrusts and thrust reversal.

Design of the First Prototype

To be able to achieve an equilibrium of forces at all possible orientations, it is crucial to be able to reverse the sign of each thrust vector. Consequently, untwisted 5-inch (127.0 mm) diameter propellers with symmetrical airfoils, so-called three-dimensional (3D) propellers of the type Gemfan 513D were used. The six motors of the type EMAX 2306 2400 kV are controlled by two Holybro Tekko32 F3 Metal 65A 4-in-1 ESC motor controllers running the firmware BLHeli32. This firmware offers the possibility to reverse the motor direction at low latency (see Figure 5).

To mount the electrical components as well as the flight controller and battery, an octahedral element was designed and placed diagonally in the middle of the airframe. Therefore, a centerpiece and six corners were 3D printed and connected with eight triangles, manufactured from the carbon fiber–reinforced plastic (CFRP) board with a thickness of 1.5 mm. The triangles include threads for nylon screws to mount the PCBs and through holes to mount the outer airframe (see Figure 4). The outer airframe consists of 3 mm/2 mm CFRP tubes and 3D-printed connectors.

The right side of Figure 4 shows the finished prototype at an empty weight of 651 g. The used computer-aided design (CAD) model is highly detailed and contains also dummy elements with the correct mass for all components.

For flight control a Holybro "Pixhawk 4 Mini" flight controller was used in combination with the open-source firmware PX4.

The PX4 firmware is modular [13] and widely used in research groups all over the world. The creators of PX4 also

FIGURE 4 Lynchpin prototype.

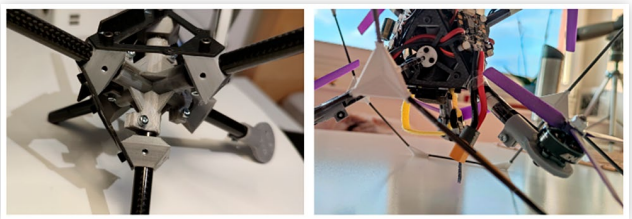

© Tangential Flight Corporation

developed the Micro Air Vehicle Link (MAVLink) protocol [14], which is essential to transmit commands to the vehicle and receive live data. The only two open-source UAV autopilot software projects that make use of the MAVLink protocol are PX4 and ArduPilot. In [15] a comparison between the two shows that PX4 has a higher number of closed issues and consequently is better maintained.

System Identification

The inertia tensor of the aircraft and the CG position could be gained from the detailed CAD model (compare Figure 3). The thrust characteristics of the propulsion system were determined with the help of the whirl tower measurements (compare [16]). The time needed to change the thrust from $T = -T_{max}$ to $T = +T_{max}$ was identified as $\tau_{max} = 0.48$ s, while the time needed to change from $T = -T_{max}/2$ to $T = +T_{max}/2$ was identified as $\tau_{half} = 0.34$ s.

As shown in Figure 5, the most latency can be addressed by the necessary change of direction of rotation since the propeller has to come to a full stop and then has to be accelerated again.

From the second law of motion in angular form, it can be seen that for a constant motor torque the change of angular speed is constant:

$$\Delta\Omega = \frac{Q}{I_{prop,zz}} \qquad \text{Eq. (11)}$$

where $I_{prop,zz}$ is the inertia of a propeller about its rotational axis. However, the thrust of a propeller is proportional to the square of the rotational speed of the propeller (compare, e.g., [11]):

$$T \propto \Omega^2 \qquad \text{Eq. (12)}$$

Consequently, for the lower range of rotational speeds, especially close to a full stop, the thrust barely changes for a certain change of rotational speed, while it always takes the same time to accomplish the same change of rotational speed, assuming a constant motor torque.

FIGURE 5 Step-response of the used propulsion system from full-negative to full-positive thrust command.

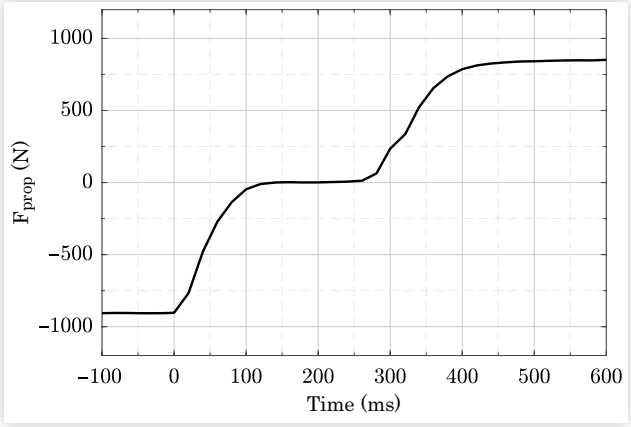

FIGURE 6 Nonlinearity of the motor output.

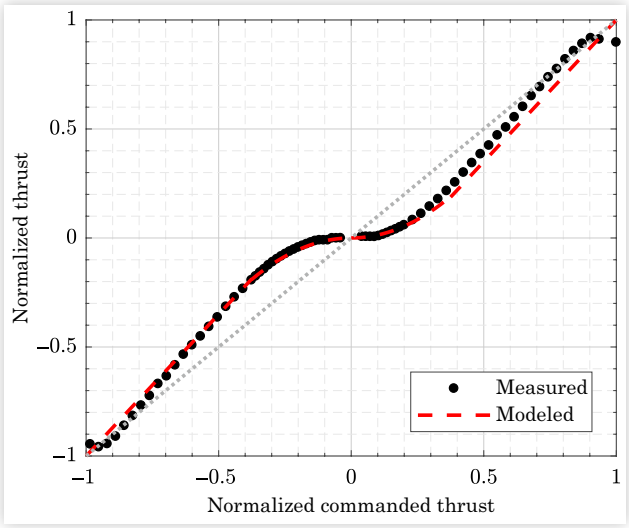

The data in Figure 6 shows that the thrust response to the motor input signal is highly nonlinear. The real behavior can be modeled with a cubic and a linear part:

$$\begin{aligned} -1.0 < m < -0.375 &: T_{norm} = 1.3(m + 0.1) + 0.17 \\ -0.375 < m < 0 &: T_{norm} = -1.35m^2 \\ 0 < m < 0.375 &: T_{norm} = 1.35m^2 \\ 0.375 < m < 1.0 &: T_{norm} = 1.3(m - 0.1) - 0.17 \end{aligned} \qquad \text{Eq. (13)}$$

where m is the normalized motor thrust input signal.

With the help of the whirl tower measurements, the torque coefficient from Equation 6 could be identified as $k_t = 0.0133\ m$ for the used propellers.

Control Strategy

The transformation in Equation 10 is fully unit related; therefore, forces and moments in *N* and *Nm* are converted to motor thrusts in *N*. However, for the flight controller, the motor outputs have to be normalized from −1 to +1.

To compensate for that fact, the following changes have been made to Equation 10:

$$\begin{bmatrix} m1 & \dots & m6 \end{bmatrix}^{\mathrm{T}} = \mathbf{M}^{-1} \begin{bmatrix} k_f F_x & k_f F_y & k_f F_z & k_m M_x & k_m M_y & k_m M_z \end{bmatrix}^{\mathrm{T}} \qquad \text{Eq. (14)}$$

where k_f and k_m are empirical factors that can be adjusted so that the aircraft will hover at a mid-thrust-stick position and have balanced flight characteristics in the roll, pitch, and yaw axes.

With Equation 14 set as a motor mixer file, the Lynchpin can already be flown as a conventional multirotor aircraft. Therefore, the inputs are set to $F_x = F_y = 0$, and M_x, M_y, and M_z are controlled by the rate controller, which processes the roll rate, pitch rate, and yaw rate setpoints coming either directly from the corresponding control sticks or the attitude controller output. F_z is controlled directly by the thrust stick.

When F_x and F_y are mapped to the roll and pitch sticks, the pilot can move tangentially in space. Therefore, M_x, M_y, and M_z are controlled by the rate controller, which gets the rate setpoints from the attitude controller with the attitude setpoints set to a constant value, e.g., from knobs at the radio. Thrust saturation was not considered in the mixing strategy so far, and during flight testing, this did not lead to any problems.

When hovering at non-zero pitch or non-zero roll attitudes, the pilot has to align the thrust vector with the roll and pitch sticks in a way that is opposed to the gravity vector. Finding this balance introduces a high pilot workload.

Consequently, for a lower pilot workload, F_x, F_y, and F_z are transformed in the earth frame. The attitude controller, used in the PX4 firmware, is completely quaternion based (compare [17]). The vehicle current attitude, calculated by the EKF state estimator, is expressed as a unit quaternion $\mathbf{q}$, which represents a rotation from the body frame (FRD—front, right, down) to the inertial frame (NED—north-east-down). The unit quaternion $\mathbf{q}$ is also referred to as a Hamiltonian attitude quaternion.

In a first step of the transformation, the heading is extracted from $\mathbf{q}$ as the Euler angle ψ. This is needed because, in manual flight mode, the pilot still expects the lateral inputs F_x and F_y to be relative to the aircraft heading. Otherwise, a forward stick input would always result in a motion toward the compass direction north.

In a second step, a new rotation quaternion $\mathbf{q_{yaw}}$ is set up that represents a rotation only about the yaw axis by $-\psi$. Furthermore, a rotation matrix $\mathbf{R_1}$ is constructed from the initial attitude quaternion $\mathbf{q}$. The columns of $\mathbf{R_1}$ are the x, y, and z aircraft body axis, expressed in the inertial frame (NED). To remove the heading influence from $\mathbf{R_1}$, these axes are now rotated with the help of $\mathbf{q_{yaw}}$ with the operation:

$$\begin{bmatrix} 0 \\ \vec{e}_i^{\,B_2} \end{bmatrix} = \mathbf{q_{yaw}} \begin{bmatrix} 0 \\ \vec{e}_i^{\,B_1} \end{bmatrix} \overline{\mathbf{q}}_{\mathbf{yaw}} \qquad \text{Eq. (15)}$$

where $\vec{e}_i^{\,B_1}$ are the aircraft body axes, expressed in the inertial frame with heading and $\vec{e}_i^{\,B_2}$ are the aircraft body axes, expressed in the inertial frame without heading. When using $\vec{e}_i^{\,B_2}$ as the columns of a second rotation matrix $\mathbf{R_2}$, we can express the rotation of the aircraft body axes from the body to the inertial frame without the heading being considered. Inverting $\mathbf{R_2}$ by building its transpose finally leads to the matrix $\mathbf{R_3} = \mathbf{R_2}^{\mathrm{T}}$. $\mathbf{R_3}$ gives the transformation of the vector $\begin{bmatrix} F_x & F_y & F_z \end{bmatrix}^{\mathrm{T}}$ from a semi-inertial frame to the body frame. In this semi-inertial frame, F_z always points up and F_x and F_y are always located in the horizontal plane, however aligned with the heading of the aircraft, so $+F_x$ is aligned with the nose of the aircraft and $+F_y$ with the right-hand side of the aircraft, in the body frame.

Consequently, the stick input force vector in the semi-inertial frame (index S) can be transformed into the body frame force vector for the motor mixer (index M) by

$$\begin{bmatrix} F_x^M & F_y^M & F_z^M \end{bmatrix}^{\mathrm{T}} = \mathbf{R_3} \begin{bmatrix} F_x^S & F_y^S & F_z^S \end{bmatrix}^{\mathrm{T}} \qquad \text{Eq. (16)}$$

This procedure works well for arbitrary roll angles and pitch angles up to $\theta = \pm 90°$. For pitch angles larger than $\theta = \pm 90°$, the heading changes its sign, and therefore, the directions of F_x^S and F_y^S also change signs. This is purely a result of the fact that the aircraft heading can only be defined as "the direction where the nose is pointing to," which does not work without singularities if the nose is pointing directly upward or downward. It does not represent a problem for the flight controller since it is completely quaternion based and does not have a gimbal lock. However, for the pilot, it can be very confusing since, at a pitch angle of slightly less than 90°, the right-hand side of the aircraft is still the same as the pilot's right-hand side, but at a pitch angle of slightly more than 90° of the right-hand side of the aircraft is the pilot's left-hand side.

This effect is illustrated in Figure 7. To compensate for this effect and enable demonstration flights with full rotations about the pitch axis, a different control mode has been implemented, where the value of ψ in $\mathbf{q_{yaw}}$ is not set constantly in real time but only once, when the aircraft is armed on the ground before takeoff.

A more intuitive way to control a 6DOF aircraft in manual flight mode would be the use of VR goggles and an axis system aligned with the pilot's view to control the thrust. Therefore, an attitude quaternion could be gained directly from the attitude of the goggles, and the "forward" would always be in the direction where the pilot is looking, while a thrust vector of $\begin{bmatrix} 0 & 0 & -mg \end{bmatrix}^{\mathrm{T}}$ in the inertial frame, as opposed to gravity, is overlaid to keep the vehicle hovering.

FIGURE 7 Heading singularity in the semi-inertial frame.

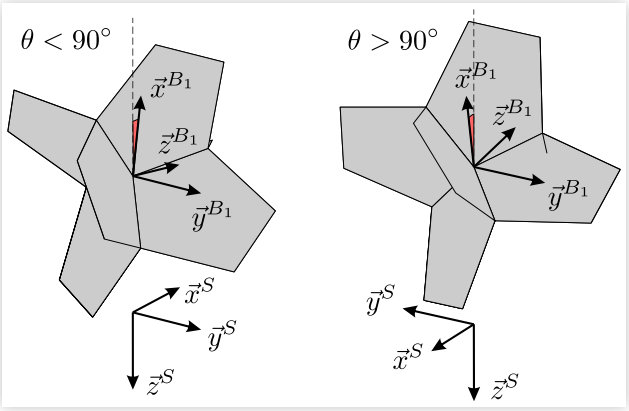

When flown in the global positioning system (GPS)-assisted flight mode (Position Hold), the transformation in Equation 16 is also used. However, the value of ψ in $\mathbf{q}_{\mathbf{yaw}}$ is set to zero because the position controller works in the inertial frame. In addition, the controller topology has to be changed. Normally, the position controller outputs a target velocity setpoint, which is then used for the velocity controller that calculates a target thrust value and an attitude setpoint in form of a quaternion $\mathbf{q}_{\mathbf{sp}}$. Consequently, the entire aircraft is tilted toward the desired direction by the attitude controller (compare [17]).

In the case of the Lynchpin, this tilt of the aircraft is not needed and also not wanted. Thus, the thrust vector output from the velocity controller $\begin{bmatrix} F_x^I & F_y^I & F_z^I \end{bmatrix}^{\mathrm{T}}$ is transformed in the body frame $\begin{bmatrix} F_x^B & F_y^B & F_z^B \end{bmatrix}^{\mathrm{T}}$ and directly forwarded to the motor mixer, while the attitude controller gets fully independent inputs.

A manual intervention is still possible in the Position Hold mode because the roll and pitch stick inputs move the GPS target setpoint in the horizontal plane in the inertial frame, while the thrust stick controls the altitude and the yaw stick controls the heading. Without pilot intervention, the aircraft will hover completely on its own, while the attitude can still be controlled, e.g., to point a rigidly mounted camera to a point of interest. The full control scheme, compared to a regular multirotor vehicle, is shown in Figure 8.

FIGURE 8 Top: Regular control scheme for a multirotor aircraft in the PX4 firmware. Bottom: Changes made for the Lynchpin drone.

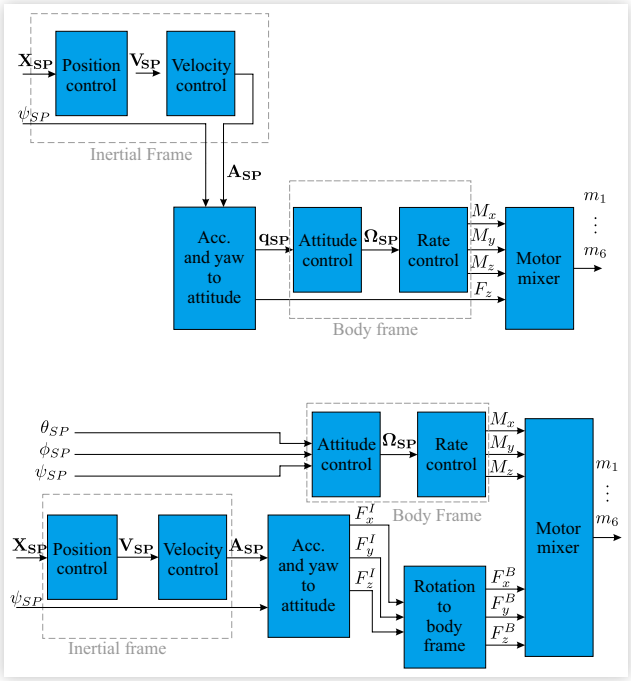

Flight Test Results

The first test flights were undertaken with manual control, and the PID values for the attitude and rate controllers were adjusted. The resulting latency from the change of direction of the motors, necessary to reverse the thrust direction, reduces the possible gains significantly. This was to be expected. For a future version of the Lynchpin, a different propulsion system with a different kind of thrust reversal method is planned to eliminate this issue.

However, also with reduced gains, the capabilities of this type of aircraft could be already demonstrated very successfully. Full rotations about the roll and pitch axis, a wall landing and different other missions have been flown (Figures 9 and 10). A flight demonstration video can be found here: https://youtu.be/bO33PNYhjFg.

In Figure 11 the recorded flight data of a slow, full rotation about the roll axis is shown. This maneuver was performed without a co-pilot in an enclosed indoor environment. Consequently, the roll rate was set to a constant value with a knob at the transmitter. It can be seen that the flight controller follows the commanded roll rate without much deviation.

During the first test flights, when flown in manual flight mode, the Lynchpin seemed to be difficult to control and could be described as "jumpy." Often, small stick inputs in F_x and F_y resulted in a sudden large displacement. This could be significantly improved when a more realistic thrust curve was added to the motor mixer code. For the implementation, the thrust model function in Equation 13 was inverted.

With this improvement it is possible for a skilled pilot to fly the Lynchpin manually in a GPS-denied environment at a very small space required and perform maneuvers such as flying through doorways and landing on a table (Figure 12). However, the handling qualities are still considered to be more difficult than for a regular drone with a higher pilot workload. This is a result of the thrust reversal latency, which still adds some level of "jumpiness" and delayed response to the flight controls.

When, for example, the direction of the commanded thrust F_x is reversed from fore to aft, several propellers have to change their directions of rotation. Consequently, for a couple of hundred milliseconds, the vehicle does not respond

FIGURE 9 The Lynchpin can fly at an arbitrary orientation.

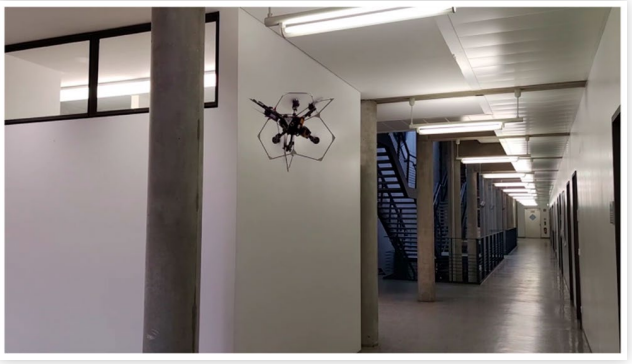

FIGURE 10 During a wall landing at $\theta = 90°$, a force $F_z^B > 0$ is used to press the Lynchpin against the wall.

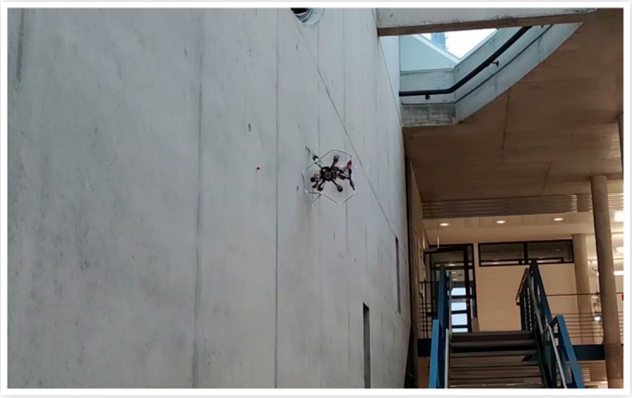

FIGURE 12 Flying in an enclosed space in a GPS-denied environment.

to the changed input of F_x; while after the propellers finished changing their direction of rotation, the new thrust direction suddenly becomes available.

It is expected that this behavior can be completely eliminated with a different propulsion system in the new version of the Lynchpin. An additional possibility to further improve the manual flight mode is an extra control loop that controls the accelerations of the vehicle in the x and y direction instead of the thrust directly.

When flown in a GPS-aided flight mode, the pilot workload is dramatically reduced. Without pilot inputs the aircraft holds its position without pilot interaction. While in an upside-down orientation, a slightly increased altitude drift could be observed. It is assumed that this is a result of the GPS with its ground plane being inverted. However, this was not critical at any point.

To reduce the pilot workload further and to make it easier to fly with the full 6DOFs, two radios and two pilots have been used, one pilot to control the aircraft position by controlling F_x, F_y, and F_z or horizontal and the vertical speeds in a GPS-aided flight and another pilot to control the rotations (compare Figure 13). For some missions the co-pilot was equipped with video goggles to operate the Lynchpin as a flying camera. This can only be described as a unique experience because one can freely look around without any angle being limited.

Figure 14 shows the recorded flight data for changes in the pitch attitude, commanded by the co-pilot. Values below or above 90° are avoided because the regular flight mode was used (compare Figure 7). The maximum flight time reached with a four-cell LiPo battery is 3 minutes and 10 seconds with a small camera module as payload.

The relatively short flight time is not only a result of the nonplanar propeller orientation but also a consequence of the small, high-speed propellers, and therefore, the flight time is expected to be significantly increased with the second version of the Lynchpin.

FIGURE 11 Flight data: A full roll flown slowly in an enclosed indoor space.

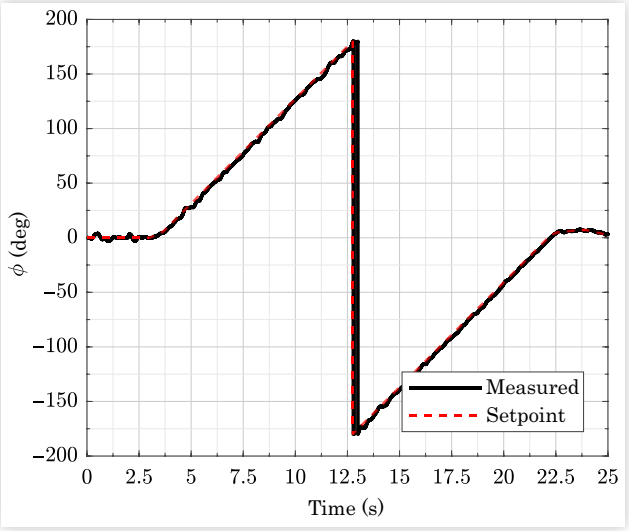

FIGURE 13 Pilot (right) and co-pilot (left) flying the Lynchpin. The pilot operates the controls for lateral movements, while the co-pilot can freely control the angles.

Possible Applications for a Single Lynchpin Aircraft

While there are disadvantages in flight time resulting from the fact that not all the thrust produced is opposed to gravity, the freedom to move and tilt independently in 3D space offers a high number of possible missions that are not feasible with conventional multirotor or helicopter aircraft.

Most relevant are aerial filming missions. While conventional systems with a gimbal are always limited in their perspective, with a 6DOF aircraft, it is possible to capture footage from any possible angle without the picture being disturbed by structural components of the airframe or propellers. In the same shot it is possible to circle around a bridge and film it from the top and the bottom seamlessly.

Other than for a filming mission, a 6DOF vehicle also has an advantage when it comes to tracking an object or a person. While with a conventional UAV, an object can simply get out of the trackable range by moving to a blind spot (e.g., exactly above the vehicle); with a 6DOF vehicle, other objects are always trackable unless they hide behind an obstacle.

For filming missions involving actors and human interactions, the geometry offers also a certain amount of protection through the outer frame surrounding the propellers, which can be further improved by the use of propeller shrouds.

In addition to pure "offline" filming missions, where the footage is saved at an onboard storage media, a 6DOF drone can introduce a unique virtual reality or augmented reality experience. This could partly be demonstrated during the first test flights with regular video goggles and a second transmitter controlling the pitch and roll angle of the aircraft.

FIGURE 14 Flight data: Pitching up and down while hovering.

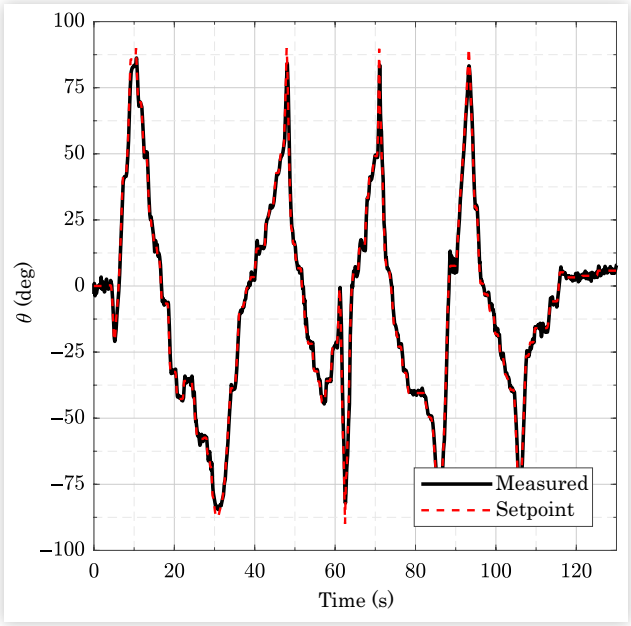

In a future version, it is planned to control the vehicle attitude with a head tracker and the translational movements with controllers or gloves. Combined with a reliable collision detection software, the operator, if not told so, would not even realize that he is flying a drone because at no point will propellers show up in the video transmission, while he is totally free to move in space.

This capability can also be utilized for building or industrial facility inspections. While this application is in general also possible with a conventional UAV and a gimbal, the Lynchpin offers complete freedom of motion without ever reaching an angle limitation that prevents the operator from moving further to the target or change the perspective.

Besides visual inspections, another large field of missions is flights incorporating a tool or a manipulator. It is possible to approach an object from any side (left, right, fore, aft, top, bottom) and at an arbitrary angle, which is a possibility that no other vehicle, besides a 6DOF aircraft, can offer. Furthermore, when touching objects, a force in an arbitrary direction can be generated (compare Figure 10).

Midair Docking of Several Lynchpin Drones

As a consequence of the highly symmetrical geometry, it is possible to attach several aircraft to each other and build modular structures in multiple ways. Two aircraft can be attached to each other in two different, mechanically stable configurations. Configuration A is shown in Figure 15 and Configuration B in Figure 16.

Due to the supersymmetrical properties of the Lynchpin, the same connection plane of the second aircraft can be connected to $N = 4$ connection planes on the first aircraft in Configuration A. In Configuration B the same connection surface group on the second aircraft, consisting of three planar surfaces, can be connected to $N = 24$ different connection surface groups on the first aircraft.

In the illustrations in Figures 15 and 16, the propeller shrouds of the Lynchpin drones have been designed in a way that they connect seamlessly. For the connection, two different surfaces at the propeller shrouds are used as shown in Figure 17. The easiest way to connect the aircraft mechanically is the use of permanent electromagnets, whose magnetism is neutralized via energization, mounted flush in the connection surfaces.

FIGURE 15 Two Lynchpin aircraft docking in Configuration A.

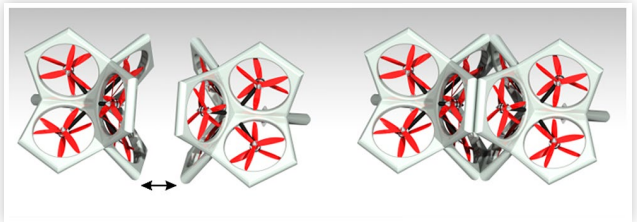

FIGURE 16 Two Lynchpin aircraft docking in Configuration B.

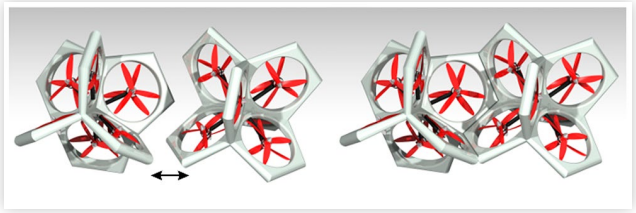

Another possibility is a slimmer design of the propeller shrouds in combination with docking connectors, placed on the corresponding surfaces as illustrated in Figure 18. Such docking connectors could also incorporate spring dampers to make the docking process smoother.

In addition, the docking connectors can also include an electrical connection, e.g., with pogo pins (compare [18]) for high-speed drone-to-drone communication or energy transmission.

The navigation during the docking process and the control of the connected group of aircraft are the subject of future research. Challenges are an exact position estimation of the neighboring aircraft as well as the decision if all group members will be controlled centrally or if there will be a master-aircraft that takes over the motor control of the other aircraft with a dynamically changed motor mixing matrix as soon as they are connected to the master.

Combined Flight Missions for Multiple Lynchpin Drones

Collaboratively using a group of aircraft is a relatively new and highly challenging field. In [19] the principle has been already demonstrated successfully. However, when using regular multirotor aircraft, where attitude and position are coupled, the docking maneuver is more difficult.

A true 6DOF flight aircraft is considered highly beneficial for midair docking maneuvers by the authors. While an approach to another aircraft in flight is difficult for a regular rotary wing aircraft because of the resulting non-zero roll and pitch angles; while moving translationally and maneuvering in space, a 6DOF vehicle can maintain fixed roll and pitch angles while maneuvering and approaching other vehicles.

FIGURE 17 Docking surfaces for both configurations.

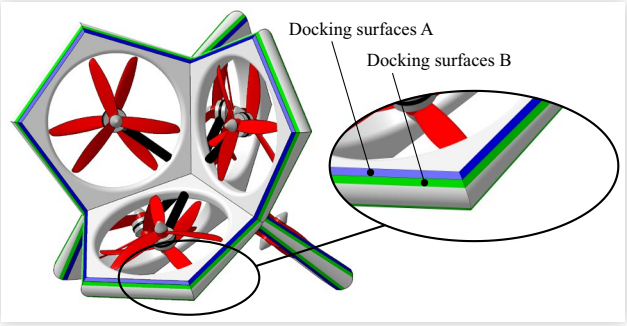

FIGURE 18 The use of external connectors with included springs dampers for softer docking maneuvers.

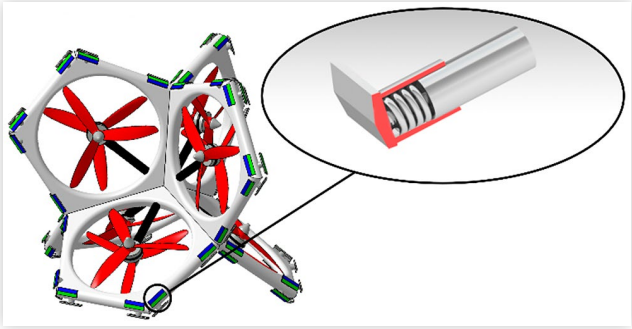

For example, when docking two regular rotary wing aircraft, while a steady wind is present, both aircraft have to be tilted permanently to generate a horizontal force, opposed to the wind. Consequently, they have to be leveled dynamically, at the last moment before they connect. With a 6DOF aircraft, the docking maneuver can be flown smoothly and purely lateral even under external disturbances.

The two basic connection Configurations A and B (compare Figures 15 and 16) offer a variety of structures that can be created in midair and a number of specific missions that are feasible. The analysis of possible missions is still the subject of ongoing research. However, some of the visions are presented here.

First of all, with four different Lynchpin aircraft, all connected in Configuration A, it is possible to grab an object from the ground or in the air, similar to what has been demonstrated in [19]. This is shown in Figure 19.

When four Lynchpin aircraft are connected in Configuration B, they can form a closed sphere; therefore, it is possible to catch flying objects (compare Figure 20) or simply place a payload inside.

With the high level of modularity and distinctive possibilities of inflight interactions, some unique missions can be mastered. This is shown in Figures 21 and 22 and [20].

FIGURE 19 Four Lynchpin aircraft forming a flying gripper.

FIGURE 20 Four aircraft connecting as a flying sphere.

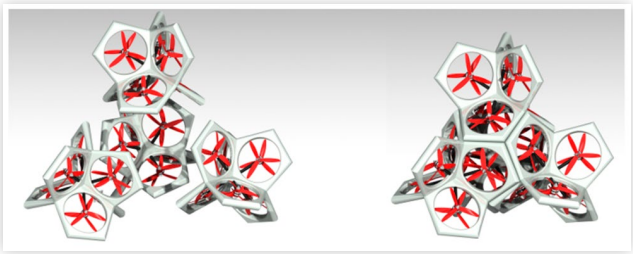

The first scenario shows the docking on a wind turbine blade for inspection and maintenance purposes. By using different formations with a different number of aircraft, it is possible to adjust the group to fit the shape of the leading edge of the turbine blade, dock there, and switch off the propulsion system completely. While such a mission would in general also be possible with a preassembled aircraft formation, which is prepared and connected on the ground, the autonomous midair docking offers a higher level of flexibility. Just in time, when one observer drone discovers a potential damage or contamination of the leading edge, the other aircraft can take the most suitable formation for docking at this specific location of the blade and dock there to finish the mission.

An additional advantage of using several independent vehicles that connect in midair is the resulting redundancy. If one aircraft fails, the docked group of aircraft can still stay airborne.

The goal of the second scenario can only be achieved with a midair docking maneuver. Imagine a very tall tree in the rainforest with little or no infrastructure at all being present in that area. A group of Lynchpin drones can approach this tree from different sides and then link together as a ring to dock to the large trunk or in a smaller group of aircraft at the top of the tree without damaging the tree. While the propulsion system is switched off completely, they remain there for several days and fulfill surveillance tasks or serve as a radio relay station or conduct air quality measurements.

FIGURE 21 Mission scenario for the modular Lynchpin aircraft: Wind turbine maintenance and inspection.

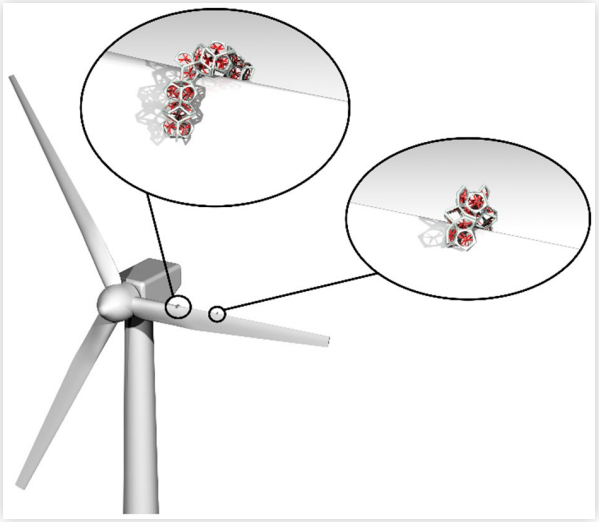

FIGURE 22 Mission scenario for a high number of modular Lynchpin aircraft: Permanent attachment to a tall tree for communication purposes.

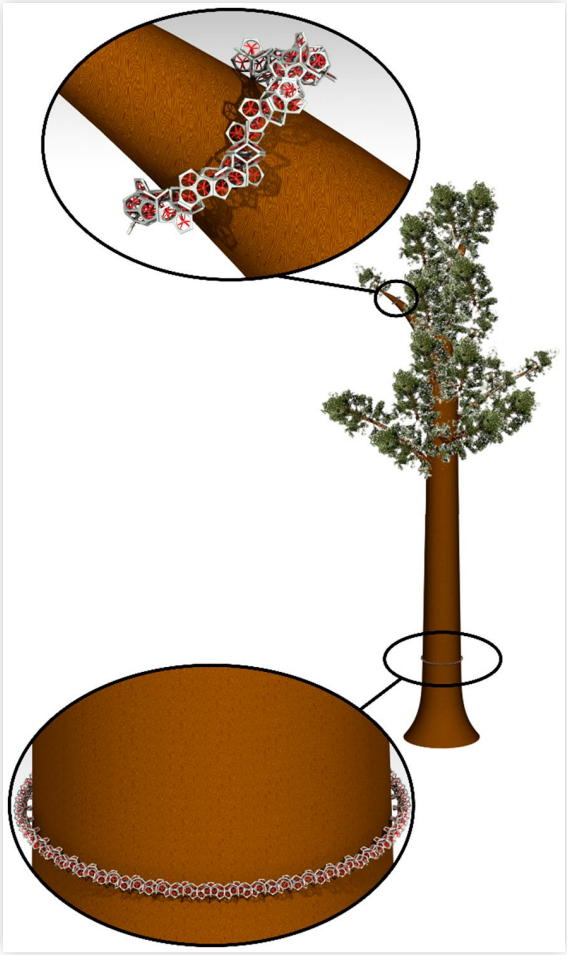

Conclusions and Outlook

A novel geometry, which is derived from particle physics, has been introduced, and its application as a modular 6DOF aircraft has been investigated theoretically and experimentally. It has been proven by practical flight tests that the proposed geometry works well for a 6DOF flight. The biggest challenge comes from the necessity to change the direction of rotation of the propellers, which results in a significant latency. However, this can be considered a general challenge, which is present for all possible 6DOF vehicle geometries using fixed propellers. In a next step, a second version of the Lynchpin aircraft will be built with a different propulsion system that is expected to completely overcome this problem.

A controller design has been presented to fly the vehicle in manual and GPS-assisted modes. Besides the latency due to thrust reversal, no principal problems for the flight controller to operate this kind of aircraft could be revealed. General challenges, when all 6DOFs have to be controlled manually have been shown, and possible solutions have been introduced successfully.

Furthermore, it has been shown that, due to its unique symmetry, the proposed geometry offers many possibilities for midair docking, which is considered to be a huge advantage in combination with the lateral flight capabilities of a 6DOF vehicle.

To investigate the possible structures that can be assembled in flight, a mathematical formulation and suitable data structure will be derived to describe the structures with a small number of parameters. In the far future possible structures should be derived in real time by the flight controller to restructure the group of aircraft flexibly during a mission.

Another imminent step in the research of the authors will be tests with a second prototype design, built in multiple numbers to investigate docking maneuvers and their feasibility. While first tests can simply be conducted in manual flight with two pilots, the possibilities to control them automatically will also be explored. Therefore, different types of distance sensors and docking clamps will be characterized for the intended use. With the aid of such sensors, new control strategies, and software solutions, the full potential of the Lynchpin drone can be exploited in the future, and the authors are excited to see the outcome of this journey.

Contact Information

T. Dashon Howard
2121 W Imperial Hwy Suite E/453
La Habra, CA 90631
tdhoward@tangentialflight.com

References

1. Hofmann L.G., Hoh, R.H., Jewell, W.F., Gary, L. et al., "Development of Automatic and Manual Flight Director Landing Systems for the XV-15 Tilt Rotor Aircraft in Helicopter Mode," NASA Technical Report No. 1092-1, 1978.
2. Molter, C. and Cheng, P.W., "ANDroMeDA—A Novel Flying Wind Measurement System," *Journal of Physics: Conference Series* 1618, no. 3 (2020): 032049, doi:10.1088/1742-6596/1618/3/032049.
3. Lawler, M., Ivler, C., Tischler, M., and Shtessel, Y., "System Identification of the Longitudinal/Heave Dynamics for a Tandem-Rotor Helicopter Including Higher-Order Dynamics," Presented at in *AIAA Atmospherics Flight Mechanics Conference and Exhibit*, Keystone, CO, 2006, doi:10.2514/6.2006-6147.
4. Brescianini, D., "Increasing the Maneuverability of Multirotor Vehicles: Attitude Control, an Omni-Directional Multirotor Vehicle, and Trajectory Generation," PhD thesis, ETH Zürich, 2018, doi:10.3929/ethz-b-000337944.
5. Ryll, M., "A Novel Overactuated Quadrotor UAV," PhD thesis, University of Stuttgart, 2015, doi:10.18419/opus-4606.
6. Howard, T., Seely, C., and Yee, J., "The Geometry of the Proton and the Tetryen Shape," Research Gate Publication, 2020, doi:10.13140/RG.2.2.25543.44964.
7. Howard, T., Systems and methods for Lynchpin structure applications. US Patent US11,117,065 B2, September 14, 2021.
8. Kamel, M. et al., "The Voliro Omniorientational Hexacopter: An Agile and Maneuverable Tiltable-Rotor Aerial Vehicle," *IEEE Robotics & Automation Magazine* 25, no. 4 (2018): 34-44, doi:10.1109/MRA.2018.2866758.
9. Company Website, "VOLIRO AG," accessed August 2022, https://voliro.com/.
10. Edmondson, A.C., *The Synergetic Geometry of R. Buckminster Fuller* (Design Science Collection, Boston, 1987), ISBN:978-1-4684-7485-5.
11. Leishman, J.G., *Principles of Helicopter Aerodynamics* (Cambridge, UK: Cambridge University Press, 2000), 43-44, ISBN:0-521-66060-2.
12. Github Repository, "PX4—Autopilot," accessed November 2021, https://github.com/PX4/PX4-Autopilot/blob/v1.11.3/src/modules/mc_hover_thrust_estimator/MulticopterHoverThrustEstimator.cpp.
13. Meier, L., Honegger, D., and Pollefeys, M., "PX4: A Node-Based Multithreaded Open Source Robotics Framework for Deeply Embedded Platforms," Presented at in *IEEE International Conference on Robotics and Automation (ICRA)*, Seattle, WA, 2015, doi:10.1109/ICRA.2015.7140074.
14. Koubâa, A., Allouch, A., Alajlan, M., Javed, Y. et al., "Micro Air Vehicle Link (MAVlink) in a Nutshell: A Survey," *IEEE Access* 7 (2019): 87658-87680, doi:10.1109/ACCESS.2019.2924410.BUGS.
15. Wang, D., Li, S., Xiao, G., Liu, Y. et al., "An Exploratory Study of Autopilot Software Bugs in Unmanned Aerial Vehicles," Presented in *Proceedings of the 29th ACM Joint Meeting on European Software Engineering Conference and Symposium on the Foundations of Software Engineering (ESEC/FSE 2021)*, Athens, Greece, 2021, doi:10.1145/3468264.3468559.
16. Molter, C. and Cheng, P.W., "Propeller Performance Calculation for Multirotor Aircraft at forward Flight Conditions and Validation with Wind Tunnel

Measurements," Presented at in *International Micro Air Vehicle Conference and Flight Competition*, Toulouse, France, 2017.

17. Brescianini D., Hehn, M., and D'Andrea, R., "Nonlinear Quadrocopter Attitude Control," Technical Report ETH Zürich, doi:10.3929/ethz-a-009970340.
18. Oung, R., Bourgault, F., Donovan, M., and D'Andrea, R., "The Distributed Flight Array," Presented at the in *IEEE International Conference on Robotics and Automation (ICRA)*, Anchorage, AK, 2010, doi:10.1109/ROBOT.2010.5509882.
19. Gabrich, B., Saldaña, D., Kumar, V., and Yim, M., "A Flying Gripper Based on Cuboid Modular Robots," Presented at in *the IEEE International Conference on Robotics and Automation (ICRA)*, Brisbane, QLD, Australia, 2018, doi:https://doi.org/10.1109/ICRA.2018.8460682.
20. Youtube Video, "Physical Simulation of Lynchpin Bonding," accessed August 2022, https://youtu.be/ZO86yAibAv0.